

NICMOS Monitoring Stability

A.B. Schultz, E. Roye, and M. Sosey
March 31, 2003

ABSTRACT

A review of the NICMOS monthly flat field monitoring data (program IDs: 9326, 9640) indicates that the NICMOS cameras are functioning as expected due in large part to the stable temperature provided by the NICMOS Cooling System (NCS). The flat field data (lamp-on) filter count rates have remained constant following SM3B/SMOV indicating that detector sensitivity and the lamps fluxes have remained constant. Additionally, pixel saturation levels have essentially remained unchanged since SMOV. The number of grot affected pixels has not changed since SMOV indicating stability within the dewar. Note that there was an increase in the number of grot affected pixels following Cycle 7 & 7N with the addition of a large chunk in the lower right quadrant of NIC1. Dithering to remove the affects of grot is recommended. A check of the NIC2 coronagraphic hole image location shows hole motion similar to what was observed during Cycle 7 & 7N. Coronagraphic observers should tailor their observations to minimize the effects of hole motion on their data. Incremental monthly and super flat field reference files have been created and delivered to the HST Archive for user support.

Introduction

The Near Infrared and Multi-Object Spectrometer (NICMOS) is a second generation Hubble Space Telescope (HST) instrument originally installed on HST during the Second Servicing Mission (SM2) during February 1997. The solid nitrogen coolant was exhausted in January 1999, shortening its useful scientific life time. NICMOS subsequently warmed up to temperatures around 260 K. With the installation of the NICMOS Cooling System (NCS) on HST during the HST Servicing Mission 3B (SM3B) in March 2002, NICMOS now operates at a temperature of ~ 77.1 K, about 15 K warmer than during Cycle 7 & 7N.

The NICMOS detectors are NICMOS3-type 256 x 256 pixel HgCdTe detectors manufactured by Rockwell. The performance of these detectors is sensitive to the operating temperature and to temperature stability. Results from the early NICMOS Servicing Mission Orbital Verification (SMOV) calibration program following SM3B indicates that the NICMOS cameras and detectors are operating quite well and within expectations (Boeker et al. 2002). In the following sections, we present the results from a monthly flat field monitor calibration program on the performance of the NICMOS cameras.

Flat Field Observations

Since NICMOS does not have a shutter, all exposures are obtained by a sequence of reset and read operations. Flat field observations are obtained by pointing HST at a blank region of the sky and obtaining exposures of each filter with the calibration lamp-off and with the lamp-on. The lamp-off observations are used to determine the thermal background at the time of the observations as well as any faint object in the field and are subtracted from the lamp-on observations to create a calibration reference file.

NICMOS has three Gilway L8010 tungsten filament calibration lamps, housed away from the Field-Offset Mechanism (FOM) to reduce thermal input to the cameras (Zaun 1994). Infrared fibers are used to transmit the light from each lamp to an integrating cavity. The integrating cavity is behind the corrector mirror at the FOM. The Pupil Alignment Mechanism (PAM) and the reimaging mirrors are not in the optical path of the beam from the integrating cavity. Light from the integrating cavity will illuminate all three detectors simultaneously. The color temperatures of the lamps are rated at 2700 K (peak wavelength 1.035 μm).

Flat Field Monitor Data

A series of flat field exposures have been obtained monthly as a part of a one orbit calibration program, early calibration program 9326 and on-going program 9640. Exposures were obtained in as many wide and medium band filters as possible for each camera. Different filters were rotated in usage from month to month. On occasion, as requested, the F160W filter exposures for each camera were driven into saturation to monitor the linearity response. The exposure times for the majority of filter observations are relatively short. The effect of these results is to produce a lower S/N calibration reference file than the STScI recommended flat field reference files used for calibration. Table 1 presents a list of the filters used for the flat field monitor programs.

Table 1. NICMOS filters used for the flat field monitor programs.

Camera							
1	F090M	F110W	F140W	F160W	F170M	-	-
2	F110W	F160W	F171M	F180M	F205W	F222M	F237M
3	F110W	F160W	F175W	F187N	F222M	F240M	-

A four point dither pattern was used for all observations. The lamp-off observations were obtained first, followed by repeating the pattern for the lamp-on observations. Camera 1 (NIC1) and Camera 2 (NIC2) flat field exposures were obtained in parallel to each other. All but a handful of Camera 3 (NIC3) observations were obtained in a separate pointing. The NIC3 flat field exposures obtained in parallel to NIC1 and NIC2 with TARG-NAME=ANY were obtained solely to monitor the respective filter count rates and were not used to create incremental flat field reference files.

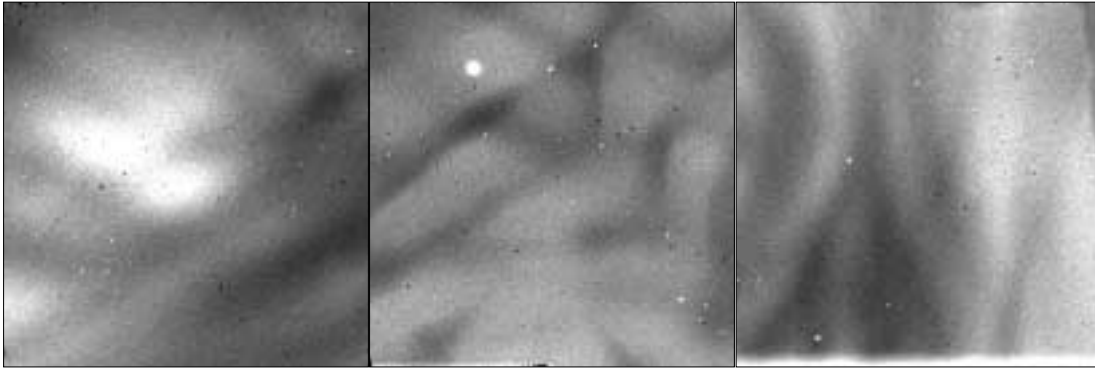
All data were retrieved from the HST Archive, and the calibration was provided by the on-the-fly processing (OTFP) or as specified in the following sections.

Morphology

Each NICMOS detector exhibits a different response to illumination from the calibration lamps which is dependent upon the wavelength response of the individual detector elements (pixels) and the luminosity and color temperature of the calibration lamps (Skinner et al. 1995, Skinner 1995). Figure 1 presents the on-orbit flat field response for the three NICMOS detectors, measured for the F160W filters (central wavelengths 1.60 μm).

The spatial structure of the flat field response has remained essentially unchanged.

Cycle 7 & 7N



Cycle 11

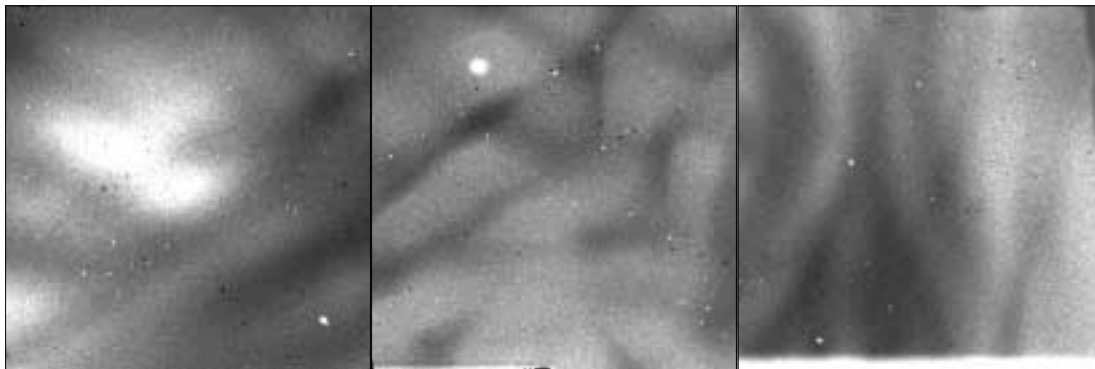


Figure 1: On-orbit flat field responses for NIC1 (left) through NIC3 (right), on a uniform grayscale. The images are inverted and dark regions have higher QE. The bands along the bottom of the NIC2 and NIC3 images, ~15-20 rows, are due to vignetting by the aperture mask on the FDA. The faint light along the upper, right edge of the NIC3 image is due to a different response in this region.

Count Rates

The count rate of lamp-on observations can be used to measure the Detective Quantum Efficiency (DQE). Changes in the count rate over time will reflect changes in the sensitivities of the detectors (Boeker et al. 2002). In the following analysis, we show that the count rates have been constant.

The IRAF task **msstatistics** was used to determine the average count rate of flat field images (lamp-on). The pipeline processed flat field observations were recalibrated using **calnica** after setting the calibration switch UNITCORR to PERFORM. A subarea of each image was used to determine the count rate to avoid vignetting at the bottom edges. For example:

```
> hedit n8i301otq_raw.fits[0] UNITCORR PERFORM ver-
```

```
> calnica n8i301otq_raw.fits "" > n8i301otq_trl.log
> msstat n8i301otq_cal.fits[1][1:256,56:256]
```

The lamp-on count rates for the selected monitor filters in each of the cameras are presented in Tables 4-6. The mean 9326 and 9640 lamp-on count rates for the F110W, F160W, and F222M filters are presented in Table 2.

Table 2. The mean lamp-on count rates (cts/sec) for selective filters.

Filter	NIC1	NIC2	NIC3
F110W	1019.16 +/- 1.66	3931.69 +/- 2.38	7459.41 +/- 23.85
F160W	438.249 +/- 0.706	1608.65 +/- 2.35	3020.00 +/- 10.38
F222M	-	249.974 +/- 1.481	1326.97 +/- 1.00

The lamp-on count rates have remained relatively constant with mean monthly variations $< 1\%$, which is due to the temperature stability provided by the NCS. This indicates that the STScI recommended flat field reference files are more than adequate to provide a good consistent calibration as provided by OTFR whenever a data set is retrieved from the HST Archive.

Linearity

The NICMOS3 detectors show non-linearity at both very small and very large total charge accumulations. The linearity curves are somewhat different for different pixels, and the saturation levels show a fairly wide dispersion. Saturation is said to be attained when 81% of the well depth is reached. The high QE pixels accumulate charge faster and so reach saturation faster than low QE pixels. Thus, the exposure times and NSAMP values selected for the linearity flat observations were chosen to yield sufficient detector reads (samples) for the high QE pixels as well as for the low QE pixels to be able to measure the linearity.

We present in Figure 2 linearity curves produced from one set of 9640 data. The determination of detector linearity is in progress and a more in depth discussion on detector linearity will be presented in a separate ISR.

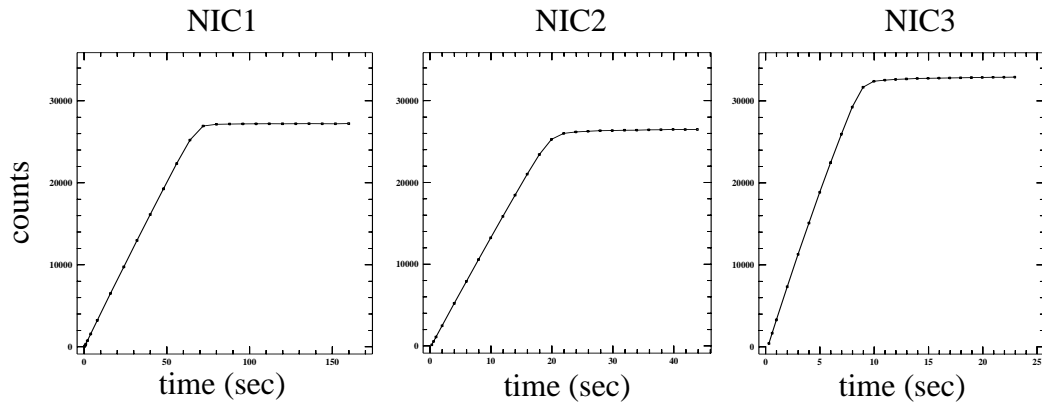


Figure 2: Response of pixel 100,100 of NIC1 (left) through NIC3 (right) to a uniform signal, illustrating the linearity behavior. The points are the observed response from the F160W filter observations; NIC1 (n8i303hfq), NIC2 (n8i303hgq), and NIC3 (n8i305onq).

Saturation Levels

The NICMOS calibration NLINCORR step applies the linearity correction to pixels with signal below their defined saturation levels. The saturation levels are in the [NODE,2] extension of the NLINFILE calibration reference file. This calibration step does not correct pixels, but rather flags them in the DQ image as saturated (DQ value = 64).

The saturation level of a given detector pixel is dependent to a large degree upon the well depth which depends upon the operating temperature. High QE pixels will saturate before low QE pixels. Thus, the monitor linearity observations can be used to check the saturation levels, and if necessary the saturation levels in the respective calibration reference files can be reset. This is a time consuming task to perform as the saturation level for each pixel has to be determined separately and the corresponding entry in the calibration reference file created. This work is in process as part of determining the linearity.

A compromise has been used for setting the saturation levels in Cycle 11 reference files. An average saturation level has been determined for each pixel and these values were entered into Cycle 7 reference files. These updated files have been delivered to the HST Archive and are being used in the OPUS pipeline.

A check of the saturation levels in the 9326 and 9640 linearity data shows that the saturation levels have remained relatively constant since SM3B/SMOV. No change to the existing saturation levels in the Cycle 11 reference files is needed.

Grot

Grot is thought to be small particles, possibly small paint flakes that were scraped off one of the optical baffles during the on-orbit mechanical deformation of the NICMOS dewar, that have settled on the detector surfaces. There are approximately 100-200

affected pixels in each NICMOS camera. Additional grot has collected on the detectors since Cycle 7 & 7N. NIC1 has seen the biggest increase in grot, with the addition of a large chunk in the lower right quadrant. Dither to remove grot.

The monitor flat field data were used to determine the average number of pixels affected by grot. The pipeline processed flat field observations were used. The four background (lamp-off) and four flat field (lamp-on) observations were co-added and the co-added background image was subtracted from the co-added flat field image. The resulting image was medianed with a ring filter (inner radius=2, outer radius=5) and this median image was subtracted from the pre-median flat field minus background image.

The IRAF task **imcalc** was used to set all pixels in the resulting image that were not affected by grot to a value of zero, thus creating a grot mask file. A threshold of 4 times the sigma of the mean count rate in the mask file was used to discriminate between the grot affected pixels and other pixels in the mask file. IRAF scripts were used to perform all of the processing steps discussed above (Sosey 2002). The number of grot affected pixels per camera is presented in Table 3.

Table 3. The number of grot affected pixels.

Date	Prop. ID	NIC1	NIC2	NIC3 ^a
May - Aug 2002	9326	186	297	252 (8985)
Sep - Nov 2002	9640	186	271	252 (9326 & 9640)
Dec 2002 - Feb 2003	9640	189	288	188 (9640)

a. higher noise statistics due to low number of flats. Measurement includes values from May 02 - Feb 03.

The number of grot affected pixels has remained essentially constant since reactivation of NICMOS following installation of the NCS.

Incremental Flat Fields

The monitor data were used to create incremental flat fields (delta flats) using an identical process to that used for creating the calibration reference files. Since only four observations have been co-added, the S/N of the incremental monthly flat fields is lower than that recommended for reference files (S/N ~300-400). For the non-thermal impacted filters (i.e., shortward of ~1.7 μm), the S/N for the lamp-on images would simply be the mean counts divided by the square root of the mean counts, assuming the background observations can be ignored. An estimate of the S/N for the corresponding calibration reference file would simply be the S/N for the single lamp-on observation times the square root of the number of observations used to create the flat. For example:

$$\begin{aligned} S/N &= \text{sqr}(4 \text{ obs}) \times (\text{cts/sec} \times \text{Exptime}) / \text{sqr}(\text{cts/sec} \times \text{Exptime}) \\ &= 2 \times (256.565 \times 31.959) / \text{sqr}(256.565 \times 31.959) = \sim 180 \end{aligned}$$

The calculation to determine the S/N for the thermally impacted filter flat fields is a bit more complicated as one needs to know the counts in the background images. As an example, the count rate of background observation n8i305p6q (F222M) is 13.647 +/- 1.427 cts/sec. An estimate of the S/N for the corresponding NIC3 flat field would be combined counts (lamp - bck) divided by the square root of the sum of the squares of the individual S/Ns. For example:

$$\begin{aligned} \text{combined counts} &= (1328.12 \times 3.985) - (13.647 \times 3.985) = 5238.174 \\ S/N(\text{lamp}) &= (1328.12 \times 3.985) / \text{sqr}(1328.12 \times 3.985) = 72.749 \\ S/N(\text{bck}) &= (13.647 \times 3.985) / \text{sqr}(13.647 \times 3.985) = 7.374 \\ S/N(\text{flat}) &= 2 \times 5238.174 / \text{sqr}(72.749^2 + 7.374^2) \\ &= \sim 140 \end{aligned}$$

The F160W filter linearity observations can be identified in Tables 4-6 by the NSAMP=25 value. Incremental flat fields were also created from these data. For these observations, the overexposed reads were not used when creating the calibration reference files. The keyword PIXVALUE in the data quality array (DQ) image headers was set to 64, signifying that the pixels were saturated, before calibration. For example:

```
> hedit n8i303hwq_raw.fits[DQ,17] PIXVALUE 64 ver-
n8i303hwq_raw.fits[DQ,17],PIXVALUE: 0 -> 64
n8i303hwq_raw.fits[DQ,17] updated
```

The incremental flat field reference files have been archived and are available to NICMOS observers. A list of the 9326 and 9640 incremental flat field reference files can be found on the NICMOS web page.

IRAF determined location of the NIC2 coronagraphic hole

NICMOS coronagraphic imaging capability is provided by a hole in the NIC2 Field Divider Assembly (FDA) mirror face in combination with the cold mask. The location of the coronagraphic hole image in NIC2 images during Cycle 7 & 7N was determined to move ~0.25 pixel in a time span of 3 orbits. Over a span of days, this migration of the hole position was about a 1-pixel locus of points. Though the movement of the coronagraphic hole during a single orbit is quite small, it was sufficient enough to require shifting of one coronagraphic image to another for PSF subtraction (Schultz et al. 1998).

The IRAF task **center** was used to determine the centroid of reversed hole images. The pipeline processed flat field observations (lamp-on) were inverted by subtracting them from a large number to make the hole positive. For example:

```
> msarith 6000.0 - n8i306wwq_cal.fits n8i306wwq_flip
> center n8i306wwq_flip.fits[1] coord=hole.lis out=n8i306wwq.da
```

Once the IRAF positions of the hole have been determined, the values need to be converted into detector coordinates, by subtracting them from 256.5, before a comparison with the Cycle 7 and 7N positions can be performed. For example:

```
Det-x = 256.5 - IRAF-y
Det-y = 256.5 - IRAF-x
```

The inferred detector and IRAF positions of the coronagraphic hole are presented in Table 7. A graphical comparison between the hole positions in Cycle 7 & 7N and Cycle 11 is presented in Figure 3. The Cycle 7 & 7N positions were obtained from coronagraphic ACQ observations and not from flat fields as are the Cycle 11 positions. Though there are only a few Cycle 11 positions plotted from the monitor data, a trend in the hole motion is evident. The hole motion is in the same general direction as was observed in Cycle 7 & 7N. The center of the movement has shifted down by ~2 pixels in Det-y. See comparison Figure 5.3, NICMOS Instrument Handbook.

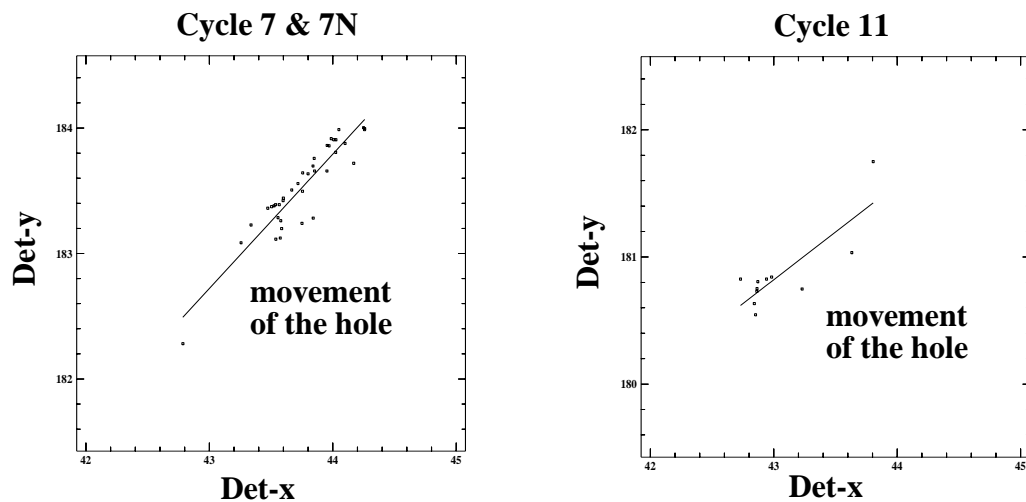


Figure 3: Coronagraphic hole locations. The detector positions of the hole image during Cycle 7 & 7N and Cycle 11 are presented for comparison. The average movement in the position of the hole image over time is represented by the lines in both plots. The hole motions are cyclic about these lines.

During Cycle 7, the cold well got pushed forward, and then slowly drifted back from this position. The image of the coronagraphic hole on the detector mimicked this motion with a long, cyclic motion. About this motion, the hole position jittered which was possibly due to bulk motion of the dewar relative to the fore optics.

The positions of the hole image in the Cycle 11 flat field monitor data shows movement similar to what was observed during Cycle 7 & 7N. This motion is on the same time scale, magnitude, and with similar jitter. This indicates that the motion is due to causes such as movement of the optical bench within the dewar and/or of the NICMOS fore optics as suggested in NICMOS Instrument Science Report ISR-99-006 (Schultz et al. 1999).

Conclusions and Recommendations

A series of flat field exposures, lamp-off and lamp-on observations, have been obtained in each camera as part of monthly monitor calibration programs 9326, which has completed, and the on-going program 9640. Exposures were obtained in a selection of wide and medium band filters. Long F160W filter exposures driven into saturation were obtained in each camera to monitor the linearity response. These data have also be used to check and set the saturation levels for each camera.

The spatial structure of the flat field response has remained essentially unchanged. The lamp-on count rates have remained relatively constant with the mean monthly variations within $< 1\%$. The saturation levels for each detector have remained relatively constant and no change to the reference file values was necessary. The determination of detector linearity is in progress and will be discussed in a separate ISR.

Monthly incremental calibration reference files have been created and delivered to the HST Archive. The S/N ($=100$ to 200) for these flat fields depends on the filter and the corresponding detected counts. They are available to those NICMOS observers who would like to calibrate their data with a flat obtained close in temperature to their observations. Super flat fields have also been created from the monitor data and are available from the Archive. A list of the 9326 and 9640 incremental and super flat field reference files can be found on the NICMOS web page.

The number of grot affected pixels has remained essentially constant since reactivation of NICMOS following installation of the NCS. As noted above, there was an increase in the number of grot affected pixels following Cycle 7 & 7N with the addition of a large chunk in the lower right quadrant of NIC1. For extended targets, dither appropriately to be able to replace the grot affected pixels with good flux values.

The position of the NIC2 coronagraphic hole image shows movement similar to what was observed during Cycle 7 & 7N and in the same general direction. The center of the movement has shifted down by ~ 2 pixels in Det-y. This suggests that the hole motion is due to causes such as movement of the optical bench within the dewar and/or of the NICMOS fore optics as suggested in NICMOS Instrument Science Report ISR-99-006

(Schultz et al. 1999). Coronagraphic observers should roll the telescope about point sources within a single orbit for companion searches. In addition, coronagraphic images of PSF stars should be obtained close in time to science observations.

References

Boeker, T., Bergeron, L.E., Mazzuca, L., Sosey, M., and Xu, C. 2002, "NICMOS Detector Performance in the NCS era," in 2002 HST Calibration Workshop, ed. S. Arribas, A. Koekemoer, and B. Whitmore, Space Telescope Science Institute, Baltimore Maryland.

Schultz, A.B., Noll, K., Storrs, A., Bacinski, J., Baggett, W., and Fraquelli, D. 1998, NICMOS Instrument Science Report, "NICMOS Camera 2 Coronagraphic ACQs," ISR NICMOS-98-012, STScI, Baltimore, MD.

Schultz, A.B., Storrs, A.D. and Fraquelli, D. 1999, NICMOS Instrument Science Report, "NICMOS Coronagraphic Imaging Strategy," ISR NICMOS-99-006, STScI, Baltimore, MD.

Skinner, C.J., Mentzell, E., and Schneider, G. 1995, "Characterization of NICMOS Array Flat-field Response," ISR NICMOS-95-005, STScI, Baltimore, MD.

Skinner, C.J. 1995, "Effects of the NICMOS Array Flat-field Response on Observations," ISR NICMOS-95-006, STScI, Baltimore, MD.

Sosey, M. 2002, "Updating the NICMOS Static Bad Pixel Masks," ISR-NICMOS-02-001.

Zaun, N. 1994, "Design of the Internal Calibration Source," OPT-151, Ball Aerospace Systems Division, Boulder, CO.

Table 4. . NICMOS Camera 1 filter count rates (Lamp=FLAT1). Obs. are the first of our images.

Filter	cts/sec	stddev	Date-Obs	SAMP_SEQ NSAMP	Exptime	Obs.
F090M	256.565	68.7932	2003-02-04	STEP8/9	31.959	n8i306wqq
F110W	1018.56	253.804	2002-05-30	STEP2/8	9.966	n6ki01uzq
	1021.92	256.822	2002-08-19	STEP2/8	9.966	n6ki04giq
	1020.61	256.152	2002-09-18	STEP2/8	9.966	n6ki05tjq
	1018.17	255.584	2002-09-10	STEP2/8	9.96	n8i301osq
	1016.31	256.020	2002-12-18	STEP2/8	9.966	n8i304y3q
	1019.38	257.31	2003-01-09	STEP2/8	9.966	n8i305pvq
F140W	1100.14	251.899	2002-06-03	STEP2/8	9.966	n6ki02azq
	1102.15	253.275	2002-10-19	STEP2/5	3.984	n8i302o2q
F160W	438.769	91.459	2002-05-30	STEP8/8	23.965	n6ki01vmq
	439.917	91.6277	2002-06-03	STEP2/8	23.965	n6ki02bmq
	438.224	91.8986	2002-07-16	STEP8/25	159.856	n6ki03l3q
	437.918	91.6986	2002-08-19	STEP8/8	23.965	n6ki04gfq
	438.696	91.7561	2002-09-18	STEP8/8	23.965	n6ki05u6q
	438.263	91.6115	2002-09-10	STEP8/8	23.965	n8i301pgq
	438.514	91.7018	2002-10-19	STEP2/10	13.954	n8i302o1q
	437.269	91.517	2002-11-08	STEP8/25	15.985	n8i303h3q
	437.947	91.601	2002-12-18	STEP8/8	23.965	n8i304yqq
	437.301	91.678	2003-01-09	STEP8/8	23.965	n8i305psq
	437.931	91.932	2003-02-04	STEP8/8	23.965	n8i306xgq
F170M	199.158	39.6982	2002-07-16	STEP8/9	31.959	n6ki03n5q
	198.175	39.570	2002-10-19	STEP8/9	31.959	n8i302n4q
	199.143	39.6412	2002-11-08	STEP8/9	31.959	n8i303ilq

Table 5. . NICMOS Camera 2 filter count rates (Lamp=FLAT1). Obs. are the first of four images.

Filter	cts/sec	stddev	Date-Obs	SAMP_SEQ NSAMP	Exptime	Obs.
F110W	3930.74	547.195	2002-05-30	STEP1/5	2.988	n6ki01v1q
	3928.55	547.339	2002-09-18	STEP1/5	2.988	n6ki05tlq
	3932.41	552.545	2002-09-10	STEP1/5	2.988	n8i301ouq
	3935.07	550.238	2002-12-18	STEP1/5	2.988	n8i304y5q
F160W	1610.76	167.790	2002-05-30	STEP1/7	4.983	n6ki01v0q
	1607.98	189.173	2002-06-03	STEP1/7	4.983	n6ki02b0q
	1604.45	168.384	2002-07-16	STEP2/25	43.864	n6ki03m0q
	1606.67	168.286	2002-09-18	STEP1/7	4.983	n6ki05tkq
	1608.22	168.314	2002-09-10	STEP1/7	4.983	n8i301otq
	1613.36	169.207	2002-10-19	STEP2/6	5.978	n8i302n7q
	1608.87	168.785	2002-11-08	STEP2/25	43.864	n8i303hgq
	1609.38	168.806	2002-12-18	STEP1/7	4.983	n8i304y4q
	1608.14	169.441	2003-02-04	STEP1/7	4.983	n8i306wwq
F171M	261.219	24.864	2002-07-16	STEP16/10	63.951	n6ki03n3q
	262.129	24.950	2002-10-19	STEP8/8	23.965	n8i302n6q
	261.662	24.900	2002-11-08	STEP16/10	63.951	n8i303ijq
F180M	225.850	20.699	2002-08-19	STEP16/10	63.951	n6ki04geq
	227.410	20.729	2002-10-19	STEP8/8	23.965	n8i302o0q
	226.303	20.726	2003-01-09	STEP16/10	63.951	n8i305prq
F205W	1406.12	143.373	2002-06-03	STEP1/7	4.983	n6ki02b1q
F222M	248.813	17.638	2002-05-30	STEP8/9	31.959	n6ki01vlq
	249.023	17.724	2002-06-03	STEP8/9	31.959	n6ki02blq
	251.773	17.940	2002-07-16	STEP8/9	31.959	n6ki03m2q
	249.167	17.704	2002-09-18	STEP8/9	31.959	n6ki05u5q
	249.010	17.6362	2002-09-10	STEP8/9	31.959	n8i301pfq
	253.089	18.0387	2002-11-08	STEP8/9	31.959	n8i303hiq
	249.810	17.719	2002-12-18	STEP8/9	31.959	n8i304ypq
	249.111	17.702	2003-02-04	STEP8/9	31.959	n8i306xfq
F237M	240.408	11.5583	2003-02-04	STEP8/8	23.965	n8i306wtq

Table 6. . NICMOS Camera 3 filter count rates. Obs. are the first of four images.

Filter	cts/sec	stddev	Date-Obs	SAMP_SEQ NSAMP	Exptime	Obs.	Lamp
F110W	7469.87	1517.60	2002-05-30	SCAMRR/7	1.421	n6ki01wgq	2
	7496.20	1514.95	2002-08-19	STEP1/6	3.985	n6ki04f6q	2
	7471.22	1522.98	2002-09-18	SCAMRR/7	1.421	n6ki05uxq	2
	7457.00	1518.11	2002-09-10	SCAMRR/7	1.421	n8i301q7q	2
	7421.07	1529.12	2002-12-19	SCAMRR/7	1.421	n8i304zxq	2
	7441.11	1528.34	2003-01-09	STEP1/6	3.985	n8i305owq	2
F160W	3027.44	512.869	2002-05-30	STEP1/5	2.988	n6ki01vyq	2
	3036.01	514.367	2002-06-03	STEP1/5	2.988	n6ki02cpq	2
	3026.78	512.175	2002-08-19	STEP1/25	22.941	n6ki04exq	2
	3025.20	513.893	2002-09-18	STEP1/5	2.988	n6ki05upq	2
	3027.23	513.525	2002-09-10	STEP1/5	2.988	n8i301pzq	2
	3014.43	513.335	2002-10-19	STEP1/5	2.988	n8i302pxq	2
	3009.84	512.122	2002-12-19	STEP1/5	2.988	n8i304z5q	2
	3002.34	509.922	2003-01-09	STEP1/25	22.940	n8i305onq	2
	3010.70	514.531	2003-02-04	STEP1/5	2.988	n8i306xuq	2
F175W	7095.13	1182.78	2002-10-19	SCAMRR/7	1.421	n8i302q7q	2
	7079.47	1186.69	2003-02-04	SCAMRR/7	1.421	n8i306ydq	2
F187N	261.126	40.201	2002-07-16	STEP16/10	63.951	n6ki03m1q	1
	260.936	40.074	2002-11-08	STEP16/10	63.951	n8i303hhq	1
F222M	1328.17	173.625	2002-06-03	STEP1/5	2.988	n6ki02cyq	1
	1325.85	173.411	2002-07-16	STEP1/6	3.985	n6ki03n6q	1
	1326.69	173.118	2002-08-19	STEP1/6	3.985	n6ki04ghq	1
	1326.02	172.932	2002-11-08	STEP1/6	3.985	n8i303imq	1
	1328.12	173.34	2003-01-09	STEP1/6	3.985	n8i305puq	1
F240M	1605.99	108.622	2002-07-16	STEP1/6	3.985	n6ki03n7q	1
	1598.58	107.731	2002-08-19	STEP1/6	3.985	n6ki04ggq	1
	1613.15	108.232	2002-11-08	STEP1/6	3.985	n8i303inq	1
	1607.21	108.304	2003-01-09	STEP1/6	3.985	n8i305ptq	1

Table 7. Locations of the coronagraphic hole. The positions are presented in detector (Det) and in image (IRAF) coordinates. The x- and y-positions are the mean of four measurements.

Prop.ID (visit)	Det-x (pixel)	Det-y (pixel)	IRAF-x (pixel)	IRAF-y (pixel)	Filter	Date
9326 (1)	42.842 +/- 0.210	180.633 +/- 0.149	75.867 +/- 0.149	213.657 +/- 0.210	F160W	2002-05-30
9326 (2)	42.730 +/- 0.132	180.826 +/- 0.029	75.674 +/- 0.029	213.768 +/- 0.132	F160W	2002-06-03
9326 (3)	43.632 +/- 0.49	181.034 +/- 0.156	75.466 +/- 0.156	212.868 +/- 0.497	F160W	2002-07-16
9326 (4)	43.805 +/- 0.281	181.750 +/- 0.496	74.759 +/- 0.496	212.695 +/- 0.281	F180M	2002-08-19
9326 (5)	42.941 +/- 0.100	180.826 +/- 0.017	75.674 +/- 0.017	213.559 +/- 0.100	F160W	2002-09-18
9640 (1)	42.870 +/- 0.003	180.805 +/- 0.002	75.695 +/- 0.002	213.63 +/- 0.003	F160W	2002-09-10
9640 (2)	42.864 +/- 0.003	180.751 +/- 0.010	75.749 +/- 0.010	213.636 +/- 0.003	F160W	2002-10-19
9640 (3)	42.862 +/- 0.003	180.730 +/- 0.008	75.770 +/- 0.008	213.638 +/- 0.003	F160W	2002-11-08
9640 (4)	42.852 +/- 0.004	180.545 +/- 0.009	75.955 +/- 0.009	213.648 +/- 0.004	F160W	2002-12-18
9640 (5)	43.229 +/- 0.342	180.748 +/- 0.048	75.752 +/- 0.048	213.271 +/- 0.342	F180M	2003-01-09
9640 (6)	42.982 +/- 0.017	180.842 +/- 0.003	75.658 +/- 0.003	213.518 +/- 0.017	F160W	2003-02-04